ACCOUNTS
of chemical research

Magic-Angle-Spinning NMR Techniques for Measuring Long-Range Distances in Biological Macromolecules

MEI HONG* AND KLAUS SCHMIDT-ROHR
Department of Chemistry and Ames Laboratory, Iowa State University, Ames, Iowa 50011, United States

RECEIVED ON OCTOBER 25, 2012

CONSPECTUS

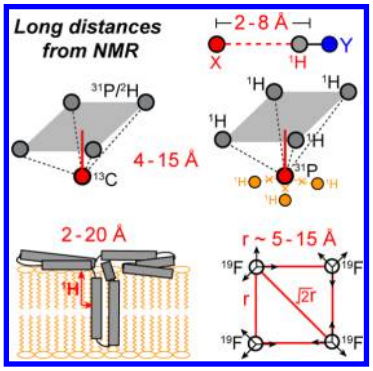

The determination of molecular structures using solid-state NMR spectroscopy requires distance measurement through nuclear-spin dipole−dipole couplings. However, most dipole-coupling techniques compete with the transverse (T_2) relaxation of the nuclear spins, whose time constants are at most several tens of milliseconds, which limits the ability to measure weak dipolar couplings or long distances.

In the last 10 years, we have developed a number of magic-angle-spinning (MAS) solid-state NMR techniques to measure distances of 15−20 Å. These methods take advantage of the high gyromagnetic ratios of ^{1}H and ^{19}F spins, multispin effects that speed up dipolar dephasing, and ^{1}H and ^{19}F spin diffusion that probes distances in the nanometer range. Third-spin heteronuclear detection provides a method for determining ^{1}H dipolar couplings to heteronuclear spins. We have used this technique to measure hydrogen-bond lengths, torsion angles, the distribution of protein conformations, and the oligomeric assembly of proteins. We developed a new pulse sequence, HARDSHIP, to determine weak long-range ^{1}H-heteronuclear dipolar couplings in the presence of strong short-range couplings. This experiment allows us to determine crystallite thicknesses in biological nanocomposites such as bone. The rotational-echo double-resonance (REDOR) technique allows us to detect multispin ^{13}C−^{31}P and ^{13}C−^{2}H dipolar couplings. Quantitative analysis of these couplings provides information about the structure of peptides bound to phospholipid bilayers and the geometry of ligand-binding sites in proteins.

Finally, we also use relayed magnetization transfer, or spin diffusion, to measure long distances. z-Magnetization can diffuse over several nanometers because its long T_1 relaxation times allow it to survive for hundreds of milliseconds. We developed ^{1}H spin diffusion to probe the depths of protein insertion into the lipid bilayer and protein−water interactions. On the other hand, ^{19}F spin diffusion of site-specifically fluorinated molecules allowed us to elucidate the oligomeric structures of membrane peptides.

1. Introduction

An essential element in solid-state NMR-based structure determination is distance measurement through nuclear-spin dipole−dipole couplings. The internuclear dipolar coupling ω_d scales with the gyromagnetic ratios (γ) of the two spins I and S and the inverse third power of the distance r_{IS}, $\omega_d \propto \gamma_I\gamma_S/r_{IS}^3$. For common spin-1/2 nuclei in organic compounds, the dipolar couplings for a 5 Å distance are, respectively, 61 Hz for ^{13}C−^{13}C, 24 Hz for ^{13}C−^{15}N, and 99 Hz for ^{13}C−^{31}P spin pairs. Since most dipolar-coupling techniques such as rotational-echo double-resonance (REDOR)[1] compete with the transverse (T_2) relaxation of the nuclear spins, whose time constants are at most several tens of milliseconds, the ability to measure weak dipolar couplings is intrinsically limited by the coherence lifetime of the nuclear spins.

We have developed several strategies to increase the distance reach of magic-angle-spinning (MAS) solid-state NMR. The first approach is to choose high-γ nuclear spins such as ^{1}H and ^{19}F. The main challenge in measuring distances to proton spins is that the multispin ^{1}H−^{1}H dipolar couplings in organic compounds cause very short ^{1}H T_2 relaxation times, which can be increased only by special decoupling sequences or very fast MAS. We review a REDOR technique designed to measure ^{1}H−X heteronuclear dipolar couplings up to 8 Å while suppressing the undesired ^{1}H−^{1}H couplings.[2]

Published on the Web 02/07/2013 www.pubs.acs.org/accounts
10.1021/ar300294x
© 2013 American Chemical Society

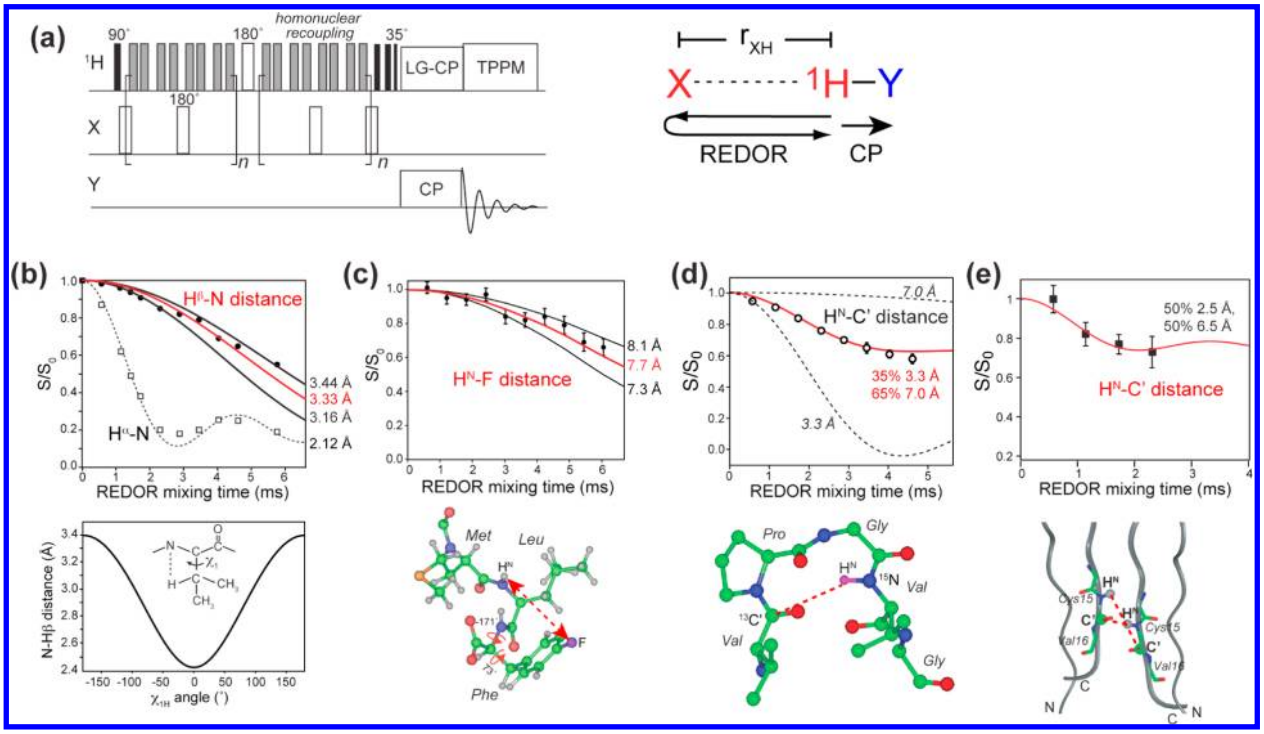

FIGURE 1. (a) Pulse sequence of the Y-detected ^{1}H–X REDOR experiment. Several applications of this method are shown in panels b–e. (b) ^{13}C-detected intraresidue Hβ–N and Hα–N REDOR dephasing in the model compound *N*-acetyl-valine.[8] The Hβ–N distance depends on the χ_1 angle as shown below the REDOR panel, where $\chi_{^1H} \equiv$ N–Cα–Cβ–Hβ = $\chi_1 - 120°$. (c) ^{15}N-detected inter-residue H^N–^{19}F REDOR dephasing of the tripeptide formyl-Met-Leu-Phe.[9] (d) ^{15}N-detected inter-residue H^N–^{13}C′ REDOR dephasing between Val6 C′ and Val9 H^N in the elastin–mimetic peptide $(VPGVG)_3$.[10] (e) Intermolecular H^N–C′ distances in Cys15 of the antimicrobial peptide, PG-1.[11] The REDOR data restrain the peptide to be parallel packed in an NCCN fashion.

The second strategy for extending the distance reach of solid-state NMR is to take advantage of multispin effects. For dipolar couplings between one X spin and multiple Y spins, the dipolar Hamiltonians for the various X–Y spin pairs commute and combine to speed up dipolar evolution, thus facilitating distance measurements. We review the principle of a multispin ^{1}H–X distance-measuring technique, HARDSHIP,[3] and show its application to biological nanocomposites. We also describe a ^{13}C–^{2}H REDOR technique for perdeuterated molecules, which can measure distances to about 7 Å.

The third strategy to measure long-range distances is to use relayed magnetization transfer, that is, spin diffusion.[4] Although semiquantitative, *z*-magnetization can diffuse over several nanometers because it can survive for hundreds of milliseconds due to the long T_1 relaxation times. We review ^{1}H and ^{19}F spin diffusion techniques that have been used successfully to determine the topology of membrane-bound peptides and proteins in lipid bilayers.[5,6]

2. ^{1}H–X Distances by REDOR

In the ^{1}H–X REDOR distance experiment (Figure 1a), ^{1}H magnetization evolves in the recoupled ^{1}H–X dipolar field. A single ^{1}H 180° pulse is applied in the center of the X–H dipolar dephasing period to refocus the ^{1}H chemical shift, while two 180° pulses per rotor period are applied to the X-spin. A homonuclear decoupling sequence is used to suppress the ^{1}H–^{1}H dipolar couplings. Therefore, the magnetization of each proton is modulated independently by its coupling to the X-spin. To detect the dipolar modulation of a specific proton, the magnetization of that proton is selectively transferred to its directly bonded spin Y, which differs from X.[2] This ^{1}H–Y transfer step can be made site-specific by using sequences that suppress ^{1}H spin diffusion. This Y-detected ^{1}H–X REDOR technique is related to the medium- and long-distance (MELODI) heteronuclear correlation experiment,[7] where the X and Y spins are the same. The use of two unlike spins for dipolar dephasing (X) and detection (Y) affords the flexibility needed to measure long distances.

As for any REDOR experiment, the distance upper limit of this Y-detected ^{1}H–X REDOR technique is dictated by the T_2 relaxation time of the evolving ^{1}H spin. Under slow MAS, the MREV-8 homonuclear-decoupled ^{1}H T_2 values are usually about 5 ms. Longer T_2 values can be achieved by using more

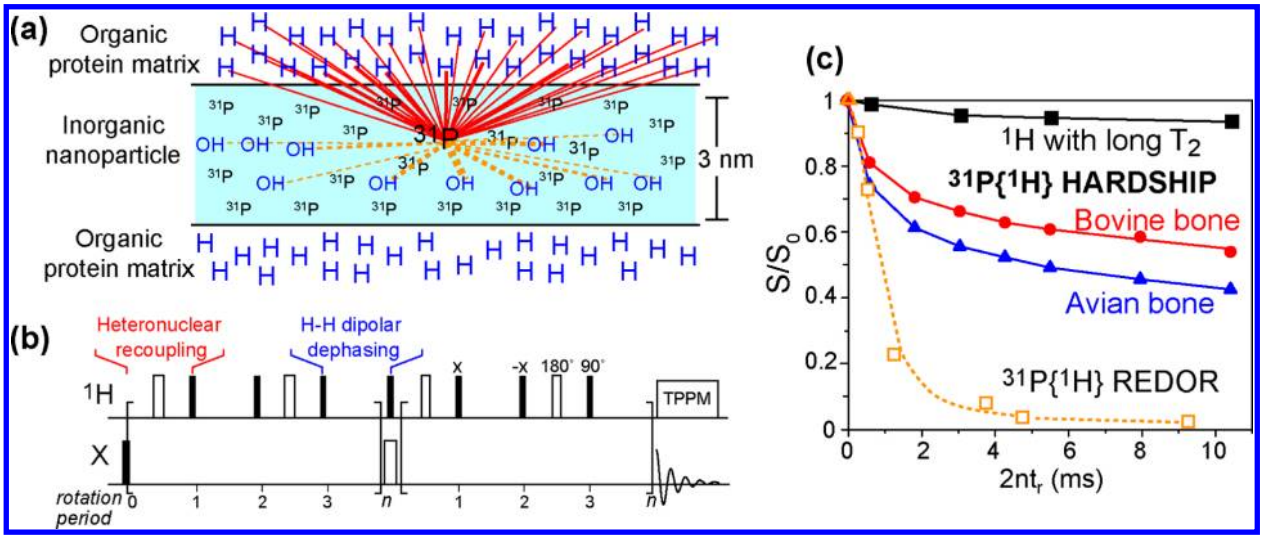

FIGURE 2. Principle and application of the HARDSHIP technique for measuring long-range distances in nanocomposites. (a) Schematic of a ^{1}H-poor inorganic nanoparticle embedded in a ^{1}H-rich organic matrix. HARDSHIP selectively probes ^{1}H−X dipolar couplings across the interface. (b) HARDSHIP pulse sequence, where ^{1}H−X heteronuclear recoupling alternates with ^{1}H−^{1}H dipolar dephasing to remove the undesired strong ^{1}H−^{31}P dipolar couplings within the inorganic phase while retaining the long-range ^{1}H−^{31}P couplings between the organic and inorganic phases. (c) Application of the HARDSHIP experiment to two bone samples with different nanocrystal thicknesses (triangles and circles) and to hydroxyapatite without an organic matrix (squares).

advanced homonuclear decoupling sequences or by reducing the ^{1}H spin density by partial deuteration.

Figure 1b−e displays some of the applications of this ^{1}H−X REDOR technique. An ^{15}N-detected H^N−CO REDOR experiment allows the measurement of hydrogen-bond lengths in suitably labeled proteins, and H^N−CO distances up to 6 Å have been measured.[2] An H^N−CO distance between Val6 and Val9 of the elastin−mimetic peptide, $(VPGVG)_3$, showed a bimodal distribution centered at 3.3 and 7.0 Å,[10] indicating that elastin adopts a mixture of a tight β-turn (35%) and an extended structure (65%) to facilitate its reversible conformational transitions. The H^N−CO distance within a residue constrains the backbone ϕ angle of that residue. This is useful for determining the conformation of glycine, where the more conventional method that correlates Cα−H dipolar coupling with the N−H^N coupling is less advantageous.[8] Similarly, side chain Hβ to backbone ^{15}Nα distances can be measured with ^{13}C detection to constrain the χ_1 torsion angle.[8]

The longest distances that can be measured with this ^{1}H−X REDOR technique are ^{1}H−^{19}F distances because of the high γ of ^{19}F spins. ^{19}F spins are usually incorporated into proteins site-specifically and are ideal distance probes. We demonstrated this technique on a *para*-^{19}F-labeled phenylalanine in the tripeptide formyl-MLF.[9] A distance of 7.7 Å was measured between 4-^{19}F-Phe and Leu H^N, which constrained the intervening phenylalanine ϕ and χ_1 torsion angles. A unique challenge of ^{1}H−^{19}F REDOR is the large chemical shift anisotropy of ^{19}F: composite pulses such as 90°225°315° are important for achieving broadband inversion of the ^{19}F polarization.

3. Multispin Distance Experiments

3.1. HARDSHIP for Biological Nanocomposites. Many hard and stiff biological materials are nanocomposites of inorganic particles embedded in an organic matrix. Examples include the load-bearing material of bone, which consists of 3-nm thick bioapatite nanocrystals in a collagen matrix (Figure 2a), dentin in teeth, with a similar overall composition, and nacre, with ~300-nm thick "bricks" of crystalline $CaCO_3$ held together by thin layers of organic "cement". Electron microscopy and scattering methods can provide information on the particle spacing and some of their dimensions, but for probing spatial variations in nanoparticle composition, interfacial structure, and other features on the 1-nm scale, solid-state NMR holds the most promise. NMR is particularly suited for studies of bone and dentin, because the nanocrystals in these materials are particularly thin (only ~3 nm) and thus less accessible to microscopy methods. At the same time, the nanosize gives a large number of spins near the organic−inorganic interfaces, which enable NMR studies of the composition and structure of organic−inorganic interfaces.

Using heteronuclear dipolar couplings, NMR can measure distances from the organic−inorganic interface to molecular

segments in both the organic matrix and the inorganic nanoparticles. With a high density of dephasing spins, for example, protons in the organic matrix, the dipolar fields are significantly stronger than a single spin pair, and dephasing at 1 nm from the interface can be significant. In fact, the dependence of the dipolar fields on the distance r from the interface is reduced to approximately $r^{3/2}$, since the number of spins with significant dipolar coupling increases with r^3.

The composition of the organic matrix near the interface is probed most easily in phosphates, where $^{13}C-^{31}P$ REDOR yields difference spectra that are dominated by the ^{13}C spins at the interface. Using this approach and spectral editing, we have shown that citrate is strongly bound to the calcium phosphate nanocrystals in bone of a wide range of vertebrate species.[12] The bound citrate provides more carboxyl groups than all noncollageneous proteins taken together. Its carboxyl−carboxyl distance favorably matches the Ca^{2+} spacing along the *c*-axis of bone apatite. This bound citrate prevents thickening of the nanocrystals by covering about 1/6 of the nanocrystal surfaces and by being too large to be incorporated into the growing crystals.

The inorganic side of the interface can be probed using long-range, multispin couplings between the abundant protons in the organic phase and X-nuclei such as ^{31}P, ^{29}Si, ^{13}C, ^{27}Al, or ^{23}Na in the inorganic phase. Quantitative analysis of the dipolar dephasing can reveal the nanoparticle thickness from the dephasing of the dominant ions, such as PO_4^{3-}, and the preferential depth of minor components from the interface.

To avoid dephasing by the strong local fields of dispersed OH or water protons in the inorganic phase, we engineered a selective pulse sequence, HARDSHIP, that achieves heteronuclear dephasing only by the organic-matrix or surface protons but not by the proximal protons in the inorganic phase. These two types of protons can be distinguished based on the strength of the $^1H-^1H$ homonuclear couplings or equivalently the transverse relaxation time, $T_{2,H}$. In this HARDSHIP experiment, heteronuclear recoupling for ~0.15 ms alternates with periods of ^1H homonuclear dipolar dephasing that are flanked by canceling 90° pulses.[3] The heteronuclear dipolar evolution of the long-$T_{2,H}$ protons is refocused within two recoupling periods (~0.6 ms). For the short-$T_{2,H}$ protons of the organic matrix, the homonuclear dipolar dephasing of transverse ^1H coherence during the period between the two 90° pulse prevents refocusing of the heteronuclear ^1H-X dipolar interaction. This results in exponential dipolar dephasing of the X-spin coherence by the organic matrix protons only. During the heteronuclear recoupling period, the strong homonuclear couplings do not affect heteronuclear dephasing, because long-range ^1H-X dipolar couplings approximately commute with short-range $^1H-^1H$ couplings. The exponential dephasing curves, reflecting ^1H-X dephasing only by the short-$T_{2,H}$ protons of the organic matrix, can be simulated accurately to take into account multispin effects, because the Hamiltonians for all heteronuclear spin pairs commute. This method was demonstrated on the bioapatite−collagen nanocomposite in bone and on pure hydroxyapatite,[3] and can be used to analyze layered structures of up to 3-nm thickness and spherical particles of up to 10-nm diameter.

3.2. $^{13}C-^{31}P$ REDOR for Membrane-Bound Peptides and Proteins. REDOR can also be used to measure distances between a single ^{13}C and multiple ^{31}P spins in phospholipid-bilayer-bound peptides and proteins. Analogous to HARDSHIP, the effect of multiple ^{31}P spins can be taken into account by geometric considerations and by numerical simulations. The average $^{31}P-^{31}P$ distance between phospholipids is about 9 Å, based on the typical phospholipid headgroup area. This separation translates to a weak $^{31}P-^{31}P$ dipolar coupling of 20 Hz, which is completely removed by MAS. Qualitatively, this means that a ^{13}C spin that is 9 Å from the ^{31}P plane will experience significant dipolar couplings to multiple ^{31}P spins, while a ^{13}C spin that is much closer to the ^{31}P plane will predominantly interact with only one ^{31}P spin. When multiple $^{13}C-^{31}P$ couplings need to be considered, the fact that they commute with each other means that the REDOR intensity, S/S_0, is the powder average of the product of the spin-pair REDOR dephasing, $(S/S_0)_{M\text{-spin-pairs}} = \langle \prod_{m=1}^{M} \cos(\bar{\omega}_{D,m} N t_r) \rangle$, where $\bar{\omega}_{D,m}$ is the time-averaged dipolar coupling of one spin pair, t_r is the MAS rotation period, and N is the number of rotation periods in the REDOR pulse train.

Multispin REDOR simulations quantitatively confirm the insight that multispin consideration is relevant only when the observed $^{13}C-^{31}P$ dipolar coupling is weak.[13] For example, for a rapid REDOR dephasing equivalent to a two-spin distance of 4.0 and 5.1 Å, which was measured for Arg11 of the antimicrobial peptide (AMP) PG-1 in POPE/POPG membranes, inclusion of a second ^{31}P spin to create a three-spin system only affected the individual $^{13}C-^{31}P$ distance modestly, to 5.2 Å each (Figure 3a, b). No additional ^{31}P spins can be included without violating the physical constraint of the $^{31}P-^{31}P$ separations in phospholipid membranes. In general, for REDOR dephasing equivalent to two-spin distances of 5 Å or longer, the inclusion of multiple ^{31}P spins increases the length of each $^{13}C-^{31}P$ vector, but

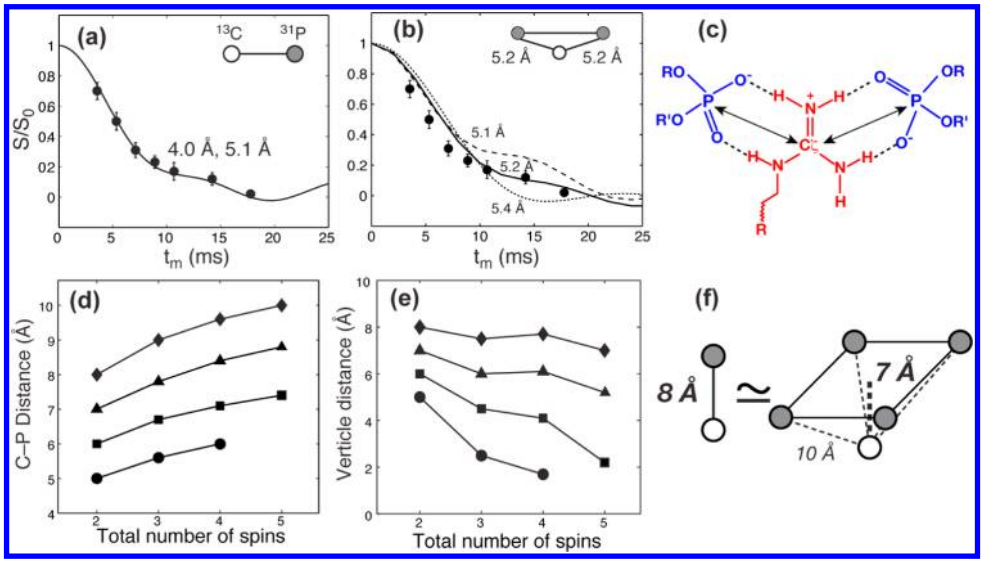

FIGURE 3. ^{13}C−^{31}P REDOR for determining protein distances to lipid ^{31}P groups. (a) REDOR dephasing of Arg11 Cζ in membrane-bound PG-1.[13] Assuming a two-spin system, the data is best fit with a 1:1 mixture of a 4.0 Å and a 5.1 Å distance. (b) Assuming two ^{31}P spins interact with Cζ at equal distances, each Cζ−P distance is 5.2 Å. (c) Guanidinium−phosphate bidentate complex, stabilized by N−H···O−P hydrogen bonds and electrostatic attraction. (d) Dependence of individual ^{13}C−^{31}P distances on the number of spins in the REDOR simulation. (e) Dependence of the vertical distance from ^{13}C to the ^{31}P plane on the number of spins in the simulation. (f) A two-spin distance of 8.0 Å is equivalent to a vertical distance of 7.0 Å in a five-spin cluster (four ^{31}P spins and one ^{13}C) in the REDOR data.

the vertical distance between ^{13}C and the ^{31}P plane increasingly approaches the nominal two-spin distance (Figure 3d−f). For example, REDOR dephasing for a nominal 8 Å spin-pair distance is equivalent to a vertical distance of 7 Å in a five-spin system.

This ^{13}C−^{31}P REDOR approach has been extensively used to study peptide−lipid interactions of arginine-rich membrane peptides.[14] These cationic peptides exhibit antimicrobial or membrane-translocation abilities. Arg-rich domains are also found in voltage-gated potassium channels where they act as the voltage sensor.[15] ^{13}C−^{31}P distances between the arginines and the lipid phosphates have provided useful mechanistic insights into how these cationic peptides bind and insert into the lipid membranes and how their orientation and depth in the membrane explain their biological function. For β-hairpin disulfide-linked AMPs such as PG-1, ^{13}C−^{31}P distances as short as 4.0 Å have been found for guanidinium Cζ (Figure 3a). The data suggests the possibility that each guanidinium can form a bidentate complex with two lipid headgroups (Figure 3b, c). Such a complex would be stabilized by N−H···O−P hydrogen bonds, as well as by electrostatic attraction. Such guanidinium−phosphate complexation can reduce the free energy of insertion of these cationic peptides into the lipid membrane. Moreover, short ^{13}C−^{31}P distances were also observed for an arginine embedded in the hydrophobic middle of the β-hairpin. Since PG-1 is known to be inserted into the hydrophobic part of the membrane based on ^{1}H spin diffusion data,[16] the short ^{13}C−^{31}P distances dictate that some lipid molecules have rotated to embed their polar headgroups into the hydrophobic region of the bilayer, which is the key structural feature of toroidal pores.[17,18]

The ^{13}C−^{31}P distances of these cationic peptides indicate that short ^{13}C−^{31}P distances are a specific feature of cationic arginine and lysine residues but not hydrophobic residues.[19] However, at physiological temperature, arginine and lysine differ in their mobilities: the guanidinium moiety is significantly less mobile than the lysine ammonium moiety, as seen in the measured order parameters. Therefore, the guanidinium ions form stable hydrogen bonds with the lipid phosphate, whereas the lysine ammonium only has transient interactions. This difference likely accounts for the more essential functional role of arginine than lysine in these cationic peptides.

3.3. ^{13}C−^{2}H REDOR for Perdeuterated Ligands. The ^{13}C−^{2}H dipolar coupling is typically too weak to be useful for measuring long distances.[20] However, the ease of perdeuteration of small molecules makes multispin ^{13}C−^{2}H REDOR a viable approach to measure much longer distances than possible by single-pair ^{13}C−^{2}H dipolar coupling. An example is given by the drug-complexed structure of the influenza virus M2 transmembrane peptide (M2TM), where the drug, amantadine, was perdeuterated.[21] In the 3-fold

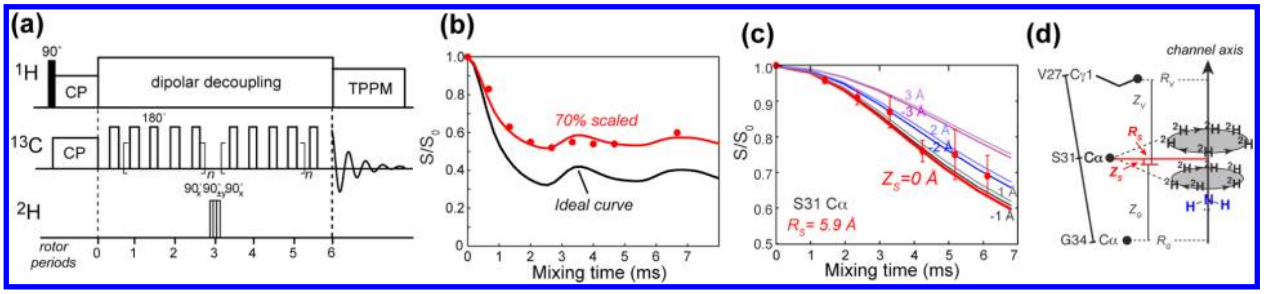

FIGURE 4. Multispin ^{13}C−^{2}H REDOR for measuring long distances.[21] (a) Pulse sequence of the ^{13}C−^{2}H REDOR experiment. (b) ^{13}C−^{2}H REDOR dephasing of ^{13}Cα,^{2}Hβ-labeled alanine. The REDOR minimum is 30% higher than the theoretical minimum due to incomplete inversion of the ^{2}H polarization. (c, d) ^{13}C−^{2}H REDOR dephasing of Ser31 Cα by perdeuterated amantadine in membrane-bound M2TM. The measured dephasing was simulated in terms of the pore radius *R* and height *Z* of the carbon from the center of the drug. The geometry is displayed in panel d.

symmetric drug, 12 C−D bonds are oriented at the tetrahedral angle of 71° from the axis of the adamantane cage, while 3 C−D bonds are parallel to the molecular axis. Each ^{13}C spin of M2TM experiences dipolar couplings to all 15 deuterons. Since the three axial deuterons are further from the surrounding peptides, a first approximation is to consider only the dipolar field of the 12 equatorial deuterons. The second moment of these 12 ^{13}C−^{2}H couplings is about 12-fold stronger than a single ^{13}C−^{2}H pair, which significantly speeds up dipolar dephasing. In the REDOR experiment, a single ^{13}C−^{2}H pair exhibits dipolar dephasing as $(S/S_0)_{1\text{-spin-pair}} = \langle 1 + 2\cos(\bar{\omega}_{CD}Nt_r)\rangle/3$, where the constant value of 1/3 results from the fact that the spin-1 deuteron causes three lines of equal intensity at 0 and $\pm\bar{\omega}_{CD}$ in its dipolar spectrum. For 12 deuterons, the REDOR dephasing is simply the product of the spin-pair dephasing, $(S/S_0)_{12\text{-spin-pair}} = 1/3^{12}\langle\prod_{m=1}^{12}[1 + 2\cos(\bar{\omega}_{CD,m}Nt_r)]\rangle$. Quantitative distance extraction for amantadine-complexed M2TM was simplified by the fast uniaxial diffusion of the drug, which allows the distances to be parametrized in terms of the pore radius and height of each ^{13}C spin from the center of the drug (Figure 4c,d). For general situations, where no symmetry is present, distances need to be quantified using additional parameters.[22]

To obtain quantitative ^{13}C−^{2}H REDOR dephasing, it is preferable to apply multiple 180° pulses on the ^{13}C spins and a single inversion pulse on the ^{2}H spin, instead of the other way around (Figure 4a), because the large ^{2}H spectral width makes it difficult to achieve complete inversion of the ^{2}H polarization by routine 180° pulses with field strengths of about 50 kHz, and cumulative incomplete inversion by multiple ^{2}H pulses will severely slow REDOR dephasing.[21] Composite pulses should be used to increase the inversion bandwidth. The degree of inversion efficiency should be calibrated using model compounds (Figure 4b).

4. Long-Range Distances from ^{1}H and ^{19}F Spin Diffusion

Direct spin diffusion among abundant and high-γ spins such as ^{1}H and ^{19}F is a powerful approach for measuring distances in the 10−20 Å range. ^{1}H spin diffusion is particularly useful for determining the immersion depth of membrane proteins in lipid bilayers.[5,6] ^{19}F spin diffusion is an elegant and background-free method for measuring site-specific distances in oligomeric protein complexes.

4.1. ^{1}H Spin Diffusion in Lipid-Bilayer Bound Membrane Peptides and Proteins. The pulse sequence for the heteronuclear-detected ^{1}H spin diffusion experiment is shown in Figure 5a. The ^{1}H magnetization of mobile lipids and water is first selected using a T_2 filter, then allowed to transfer to the ^{1}H-suppressed rigid protein during a mixing time. The result of spin diffusion is detected through the protein ^{13}C or ^{15}N signals.[5,6] Only when the protein is in close proximity to the lipid chains or water will there be a lipid−protein or water−protein ^{1}H−^{13}C cross peak. The T_2 filter requires that the experiment be conducted in the liquid-crystalline phase of the membrane where the lipid mobility is higher than the protein mobility and spin diffusion within the lipid matrix is rate-limiting, occurring on the time scale of tens to hundreds of milliseconds. Once the ^{1}H magnetization diffuses to a protein site, it will be rapidly equilibrated in the protein due to the protein's rigidity. Applied in this way, the immersion depth is not site-specific, but is the minimum distance between the protein and the hydrophobic center of the membrane. The lipid-chain-end methyl protons (0.9 ppm) are more desirable depth probes than the methylene protons due to the former's better defined locations.

Figure 5b−d shows examples of the lipid−protein ^{1}H spin diffusion experiments to determine the immersion depths of membrane proteins. Small membrane peptides such as PG-1 can adopt different insertion motifs depending on the

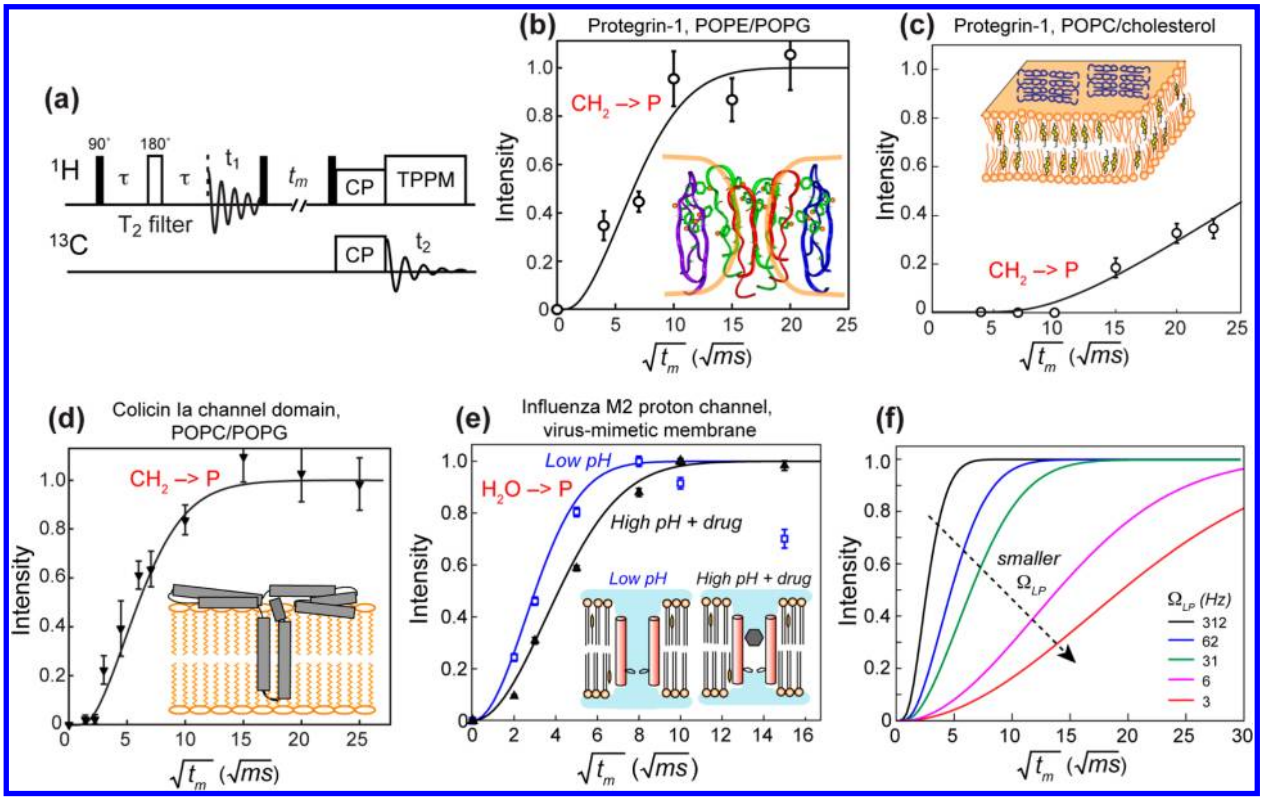

FIGURE 5. ^{1}H spin diffusion to determine depth of insertion and water interaction of membrane peptides and proteins. (a) Pulse sequence of the ^{13}C-detected ^{1}H spin diffusion experiment. (b) Lipid chain to PG-1 spin diffusion in bacteria-mimetic POPE/POPG membranes. The best-fit distance of 2 Å indicates a TM topology. (c) Lipid-chain to PG-1 spin diffusion in eukaryote-mimetic POPC/cholesterol membranes. The slow buildup rate is best fit to a 20 Å distance, indicating that PG-1 lies on the surface of this membrane. (d) Lipid chain to colicin Ia channel domain spin diffusion in POPC/POPG membranes. The fast buildup and the 2 Å distance indicates that the protein has a TM domain, thus supporting the umbrella model shown here. (e) Water spin diffusion to M2TM in two different states. The buildup is faster for the open channel at low pH than for the drug-bound closed channel at high pH (filled triangles). (f) Simulated lipid−protein spin diffusion buildup curves for various interfacial transfer rates, Ω_{LP}. In the simulations, D_P = 0.3 nm^2/ms, D_L = 0.012 nm^2/ms, and the peptide−lipid separation is fixed at 2 Å.

membrane composition:[16] it inserts into the bacteria-mimetic anionic membrane but lies on the surface of the eukaryote-mimetic membrane, which explains the selective activity of this AMP. Larger membrane proteins such as the bacterial toxin colicin Ia channel domain can possess both surface-bound and TM domains. The presence or absence of a TM domain can be unambiguously determined from the lipid−protein spin diffusion buildup curve (Figure 5d). For this toxin, the fast spin diffusion from the lipid chains supports an umbrella model while disproving a penknife model.[6]

Distance quantification of the cross peak buildup curves requires knowledge of the spin diffusion coefficients. For lipid−protein spin diffusion, the diffusion coefficients within the lipid matrix (D_L) and within the protein (D_P) are necessary.[6] For water-to-protein spin diffusion, an analogous D_W is involved. These diffusion coefficients can be estimated from the dipolar couplings of lipids, protein, and water using the relation $D = \Omega a^2$, where Ω is the dipolar coupling and a is the lattice spacing between spins. For rigid proteins, a D_P of 0.8 nm^2/ms was estimated, corresponding to a ^{1}H−^{1}H dipolar coupling of 20 kHz for a 2 Å separation. The dipolar couplings between vicinal protons of liquid-crystalline lipids correspond to a D_L of 0.01−0.03 nm^2/ms. The exact value depends on the membrane dynamics: cholesterol-rich membranes have higher rigidity and hence larger D_L, whereas low-melting phospholipid membranes such as POPC and POPG have smaller D_L's. The interfacial transfer rate, Ω_{LP}, is an important adjustable parameter in spin diffusion simulations. Ω_{LP} is small due to the low probability of intermolecular contact. It can be estimated from the shape of the observed buildup curve (Figure 5f): lower Ω_{LP} decreases the slope of the buildup curve.[16] For water−protein spin diffusion, D_W is typically 3 nm^2/ms and Ω_{WP} is about 200 Hz. Most membrane proteins exhibit rapid water−protein magnetization transfer that is equilibrated by ~100 ms. This reflects the fact that both surface-bound and TM membrane peptides have some residues exposed to water on the membrane surface.

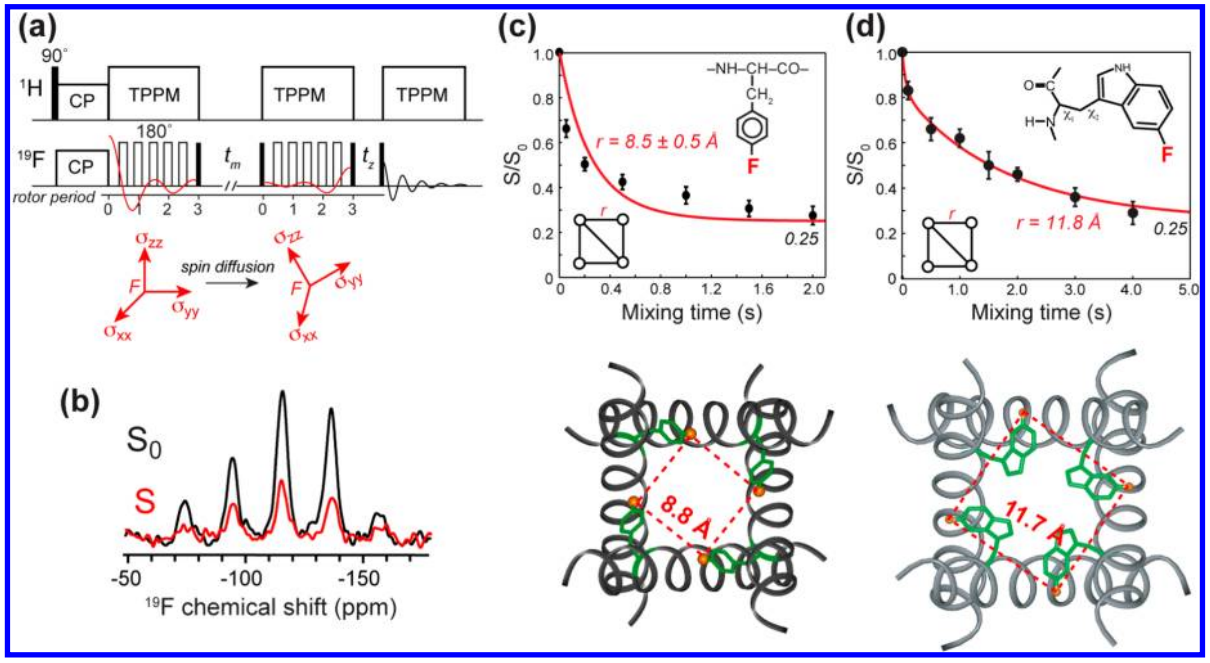

FIGURE 6. Determination of distances and oligomeric structure using ^{19}F spin diffusion. (a) ^{19}F CODEX pulse sequence.[29] Magnetization transfer to ^{19}F with a different chemical shift tensor orientation reduces the intensity of a stimulated echo. (b) Representative ^{19}F CODEX control (S_0) and exchange (S) spectra, of 4-^{19}F-Phe30 in M2TM.[30] (c) ^{19}F CODEX data of 4-^{19}F-Phe30 in M2TM. The CODEX signals decay to 0.25, proving the tetrameric nature of M2TM in the lipid bilayer. The decay rate yields a nearest-neighbor distance of 8.8 Å. (d) ^{19}F CODEX data of 5-^{19}F-Trp41 in DMPC-bound M2TM. The distance of 11.8 Å constrains both the rotameric structure of Trp41 and interhelical packing.[31]

When ^{1}H spin diffusion is used to determine the depth of membrane proteins, a 1D lattice model for magnetization transfer along the bilayer normal is the most appropriate framework. For water–protein spin diffusion, an alternative 3D lattice model can be more informative. If we assume an average diffusion coefficient D_{eff} for the entire protein–lipid–water system, then the spin diffusion buildup is proportional to the water-exposed surface area (S_{WP}) of the protein.[23,24] This approach has been used to investigate the conformational changes of ion channels and other membrane proteins. For example, the low-pH state of the influenza M2 proton channel has a faster buildup rate than the drug-bound state of the channel; the difference suggests a 2-fold larger S_{WP} in the open state of the channel (Figure 5e).[24]

A specific question about water–protein interactions is how water interacts with cationic residues in membrane-bound AMPs and cell-penetrating peptides. The ^{13}C-detected ^{1}H spin diffusion experiments revealed that the arginine guanidinium ions are well solvated by water molecules and that water–peptide spin diffusion can be observed in as short as 1 ms.[25,26] This observation, together with the short arginine–phosphate distances, supports the notion that arginines are stabilized in lipid membranes by both salt bridges and water dimples.

^{31}P-detected ^{1}H spin diffusion is also useful for understanding membrane phenomenon. Lipid chain to headgroup spin diffusion usually requires hundreds of milliseconds to equilibrate, but the presence of TM protein domains speeds up this spin diffusion by providing a rigid conduit along which magnetization transfer can occur. Therefore, even without ^{13}C-labeled proteins, one can use the ^{31}P-detected ^{1}H spin diffusion experiment to measure the depth of insertion of membrane proteins indirectly.[6] Since the membrane surface is almost always hydrated, water–^{31}P cross peaks are usually readily detectable. However, these cross peaks require exchangeable protons in the membrane, either from the lipid headgroups such as the NH_2 group in phosphatidylethanolamine or from the protein.[27] In protein-free phosphatidylcholine membranes, no water–^{31}P cross peaks can be observed, even though the membrane is hydrated.

4.2. ^{19}F–^{19}F Distances from CODEX Spin Diffusion. ^{19}F spin diffusion provides a novel method to measure distances to ~15 Å as well as to determine the oligomeric number of protein assemblies. This approach is based on the CODEX technique initially developed to measure slow reorientational motions.[28] The idea is to use rotation-synchronized 180° pulses to recouple the anisotropic ^{19}F chemical shift interaction to create a stimulated echo (Figure 6a).

The echo intensity decreases when the orientation-dependent chemical shift frequency changes due to molecular motion or magnetization transfer to another spin with a different orientation. This magnetization transfer is driven by distance-dependent dipole couplings. When spin diffusion reaches equilibrium among all spins in an *n*-spin cluster, the fraction of magnetization remaining at the original site is $1/n$, which is the equilibrium echo intensity.[29] Therefore, the CODEX intensity at equilibrium gives the oligomeric number, while the decay rate to equilibrium reveals internuclear distances. The distances can be quantified using an exchange-matrix formalism: the time-dependent magnetization, $M(t)$, follows the first-order differential equation[30] $dM(t)/dt = -\mathbf{K}M(t)$, where $\mathbf{K}$ is the *n*-dimensional exchange matrix containing rate constants k_{ij}. The rate constants depend on the dipolar coupling according to $k_{ij} = 0.5\pi \cdot \omega_{ij}^2 \cdot F_{ij}(0)$, where $F_{ij}(0)$ is the overlap integral describing the probability that single-quantum transitions occur at the same frequency for spins *i* and *j*. The overlap integral can be measured from model compounds with known $^{19}F-^{19}F$ distances. A consensus value of $F(0) = 37\ \mu s$ has been found for a MAS frequency of 8 kHz for ^{19}F spins in aromatic compounds.[30]

This ^{19}F CODEX technique has been applied to the AMP PG-1 and the influenza M2TM. It was found that PG-1 associates in two-spin clusters within a distance upper limit of 15 Å in POPE/POPG membranes.[16] The association is between like strands: the C-terminal strand with the C-terminal strand and the N-terminal strand with another N-terminal strand. Combined with other site-specific distances,[11] this result indicates that PG-1 forms membrane-spanning parallel NCCN β-barrels in bacteria-mimetic anionic membranes. In contrast, in POPC/cholesterol bilayers, PG-1 forms larger spin clusters of at least four ^{19}F spins, suggesting β-sheets. Moreover, these β-sheets lie on the membrane surface, thus explaining the selective activity of this AMP against microbial membranes.

The ^{19}F CODEX experiment was also used to measure interhelical distances in the tetrameric influenza M2TM. A *para*-fluorinated phenylalanine at residue 30 gave a nearest-neighbor distance of 8.8 Å, while 5-^{19}F-labeled Trp41 showed a nearest-neighbor distance of 11.8 Å. These distances constrained the tetramer packing as well as the rotameric conformation of Phe30 and Trp41. The latter gave useful insight into the gating mechanism of this proton channel.[31]

5. Conclusion

The above survey shows an array of techniques that are now available to measure distances up to about 15 Å. As demonstrated for PG-1 and the influenza M2 peptide, just a few sparse long-range distances can already provide powerful constraints to the three-dimensional fold of peptides and proteins. Future directions include extending these techniques to measure multiple long-range distances simultaneously in extensively labeled proteins, in order to reduce the need for site-specifically labeled samples.

M.H. is grateful to NSF for funding the majority of the techniques described in this Account. We thank NIH and DOE for supporting the applications of these methods to many interesting biological and materials problems. We also thank the many co-workers involved in these studies, especially when it was not clear that the experiments would work.

BIOGRAPHICAL INFORMATION

Mei Hong is a Professor of Chemistry at Iowa State University. She received her B.A. at Mount Holyoke College and her Ph.D. at the University of California, Berkeley. Since joining the faculty at Iowa State University in 1999, she has focused on studying membrane protein structure, dynamics, and mechanism of action using solid-state NMR.

Klaus Schmidt-Rohr is a Professor of Chemistry at Iowa State University. He received his B.S. and Ph.D. at the University of Mainz, Germany, working at the Max Planck Institute for Polymer Research. After a faculty position at the University of Massachusetts at Amherst, he joined Iowa State University in 2000. Professor Schmidt-Rohr develops and applies solid-state NMR techniques to study the structure and dynamics of complex materials.

FOOTNOTES

*To whom correspondence should be addressed. E-mail: mhong@iastate.edu.
The authors declare no competing financial interest.

REFERENCES

1 Gullion, T.; Schaefer, J. Rotational echo double resonance NMR. *J. Magn. Reson.* **1989**, *81*, 196–200.
2 Schmidt-Rohr, K.; Hong, M. Measurements of carbon to amide-proton distances by C—H dipolar recoupling with ^{15}N NMR detection. *J. Am. Chem. Soc.* **2003**, *125*, 5648–5649.
3 Schmidt-Rohr, K.; Rawal, A.; Fang, X. W. A new NMR method for determining the particle thickness in nanocomposites, using T2,H-selective X{1H} recoupling. *J. Chem. Phys.* **2007**, *126*, No. 054701.
4 Schmidt-Rohr, K.; Spiess, H. W.: *Multidimensional Solid-State NMR and Polymers*, 1st ed.; Academic Press: San Diego, CA, 1994.
5 Kumashiro, K. K.; Schmidt-Rohr, K.; Murphy, O. J.; Ouellette, K. L.; Cramer, W. A.; Thompson, L. K. A novel tool for probing membrane protein structure: Solid-state NMR with proton spin diffusion and X-nucleus detection. *J. Am. Chem. Soc.* **1998**, *120*, 5043–5051.
6 Huster, D.; Yao, X. L.; Hong, M. Membrane protein topology probed by ^1H spin diffusion from lipids using solid-state NMR spectroscopy. *J. Am. Chem. Soc.* **2002**, *124*, 874–883.
7 Yao, X. L.; Schmidt-Rohr, K.; Hong, M. Medium- and long-distance 1H-13C heteronuclear correlation NMR in solids. *J. Magn. Reson.* **2001**, *149*, 139–143.
8 Sinha, N.; Hong, M. X-1H rotational-echo double-resonance NMR for torsion angle determination of peptides. *Chem. Phys. Lett.* **2003**, *380*, 742–748.
9 Wi, S.; Sinha, N.; Hong, M. Long range $^1H-^{19}F$ distance measurement in peptides by solid-state NMR. *J. Am. Chem. Soc.* **2004**, *126*, 12754–12755.
10 Yao, X. L.; Hong, M. Structural distribution in an elastin-mimetic peptide $(VPGVG)_3$ investigated by solid-state NMR. *J. Am. Chem. Soc.* **2004**, *126*, 4199–4210.

11 Mani, R.; Tang, M.; Wu, X.; Buffy, J. J.; Waring, A. J.; Sherman, M. A.; Hong, M. Membrane-bound dimer structure of a β-hairpin antimicrobial peptide from rotational-echo double-resonance solid-state NMR. *Biochemistry* **2006**, *45*, 8341–8349.

12 Hu, Y. Y.; Rawal, A.; Schmidt-Rohr, K. Strongly bound citrate stabilizes the apatite nanocrystals in bone. *Proc. Natl. Acad. Sci. U.S.A.* **2010**, *107*, 22425–22429.

13 Tang, M.; Waring, A. J.; Hong, M. Phosphate-mediated arginine insertion into lipid membranes and pore formation by a cationic membrane peptide from solid-state NMR. *J. Am. Chem. Soc.* **2007**, *129*, 11438–11446.

14 Hong, M.; Su, Y. Structure and dynamics of cationic membrane peptides and proteins: Insights from solid-state NMR. *Protein Sci.* **2011**, *20*, 641–655.

15 Doherty, T.; Su, Y.; Hong, M. High-resolution orientation and depth of insertion of the voltage-sensing S4 helix of a potassium channel in lipid bilayers. *J. Mol. Biol.* **2010**, *401*, 642–652.

16 Mani, R.; Cady, S. D.; Tang, M.; Waring, A. J.; Lehrer, R. I.; Hong, M. Membrane-dependent oligomeric structure and pore formation of a beta-hairpin antimicrobial peptide in lipid bilayers from solid-state NMR. *Proc. Natl. Acad. Sci. U.S.A.* **2006**, *103*, 16242–16247.

17 Matsuzaki, K.; Murase, O.; Fujii, N.; Miyajima, K. An antimicrobial peptide, magainin 2, induced rapid flip-flop of phospholipids coupled with pore formation and peptide translocation. *Biochemistry* **1996**, *35*, 11361–11368.

18 Ludtke, S. J.; He, K.; Heller, W. T.; Harroun, T. A.; Yang, L.; Huang, H. W. Membrane pores induced by magainin. *Biochemistry* **1996**, *35*, 13723–13728.

19 Su, Y.; Doherty, T.; Waring, A. J.; Ruchala, P.; Hong, M. Roles of arginine and lysine residues in the translocation of a cell-penetrating peptide from ^{13}C, ^{31}P, and ^{19}F solid-state NMR. *Biochemistry* **2009**, *48*, 4587–4595.

20 Sack, I. I.; Goldbourt, A.; Vega, S.; Buntkowsky, G. Deuterium REDOR: Principles and applications for distance measurements. *J. Magn. Reson.* **1999**, *138*, 54–65.

21 Cady, S. D.; Schmidt-Rohr, K.; Wang, J.; Soto, C. S.; DeGrado, W. F.; Hong, M. Structure of the amantadine binding site of influenza M2 proton channels in lipid bilayers. *Nature* **2010**, *463*, 689–692.

22 Cady, S. D.; Wang, J.; Wu, Y.; DeGrado, W. F.; Hong, M. Specific binding of adamantane drugs and direction of their polar amines in the pore of the influenza M2 transmembrane domain in lipid bilayers and dodecylphosphocholine micelles determined by NMR spectroscopy. *J. Am. Chem. Soc.* **2011**, *133*, 4274–4284.

23 Ader, C.; Schneider, R.; Seidel, K.; Etzkorn, M.; Becker, S.; Baldus, M. Structural rearrangements of membrane proteins probed by water-edited solid-state NMR spectroscopy. *J. Am. Chem. Soc.* **2009**, *131*, 170–176.

24 Luo, W.; Hong, M. Conformational changes of an ion channel membrane protein detected through water−protein interactions using solid-state NMR spectroscopy. *J. Am. Chem. Soc.* **2010**, *132*, 2378–2384.

25 Su, Y.; Waring, A. J.; Ruchala, P.; Hong, M. Membrane-bound dynamic structure of an arginine-rich cell-penetrating peptide, the protein transduction domain of HIV TAT, from solid-state NMR. *Biochemistry* **2010**, *49*, 6009–6020.

26 Li, S.; Su, Y.; Luo, W.; Hong, M. Water-protein interactions of an arginine-rich membrane peptide in lipid bilayers investigated by solid-state nuclear magnetic resonance spectroscopy. *J. Phys. Chem. B* **2010**, *114*, 4063–4069.

27 Doherty, T.; Hong, M. 2D (1)H-(31)P solid-state NMR studies of the dependence of interbilayer water dynamics on lipid headgroup structure and membrane peptides. *J. Magn. Reson.* **2009**, *196*, 39–47.

28 deAzevedo, E. R.; Bonagamba, T. J.; Hu, W.; Schmidt-Rohr, K. Centerband-only detection of exchange: efficient analysis of dynamics in solids by NMR. *J. Am. Chem. Soc.* **1999**, *121*, 8411–8412.

29 Buffy, J. J.; Waring, A. J.; Hong, M. Determination of peptide oligomerization in lipid membranes with magic-angle spinning spin diffusion NMR. *J. Am. Chem. Soc.* **2005**, *127*, 4477–4483.

30 Luo, W.; Hong, M. Determination of the oligomeric number and intermolecular distances of membrane protein assemblies by anisotropic ^{1}H-driven spin diffusion NMR spectroscopy. *J. Am. Chem. Soc.* **2006**, *128*, 7242–7251.

31 Luo, W.; Mani, R.; Hong, M. Side-chain conformation and gating of the M2 transmembrane peptide proton channel of influenza A virus from ^{19}F solid-state NMR. *J. Phys. Chem. B* **2007**, *111*, 10825–10832.